analytical chemistry

Article

pubs.acs.org/ac

Multiplexed Detection of mRNA Using Porosity-Tuned Hydrogel Microparticles

Nak Won Choi,[†,‡,§] Jungwook Kim,[‡,#] Stephen C. Chapin,[‡] Thao Duong,[†] Elaine Donohue,[†] Pramod Pandey,[†] Wendy Broom,[†] W. Adam Hill,*[,†] and Patrick S. Doyle*[,‡]

[†]Novartis Institutes for Biomedical Research (NIBR), Cambridge, Massachusetts 02139, United States

[‡]Department of Chemical Engineering, Massachusetts Institute of Technology, Cambridge, Massachusetts 02139, United States

Supporting Information

ABSTRACT: Transcriptional profiling, which is directly or indirectly associated with expressed protein levels, has been used in various applications including clinical prognosis and pharmaceutical investigation of drug activities. Although the widely used reverse transcription polymerase chain reaction (RT-PCR) allows for the quantification of absolute amounts of mRNA (mRNA) from inputs as small as a single cell, it is an indirect detection method that requires the amplification of cDNA copies of target mRNAs. Here, we report the quantification of unmodified full-length transcripts, using poly(ethylene) glycol diacrylate (PEGDA) hydrogel microparticles synthesized via stop flow lithography (SFL). We show that PEG600 serves as an effective porogen to allow for the capture of large (~1000−3700 nt long) mRNAs. Our relatively simple hydrogel-based mRNA detection scheme uses a multibiotinylated universal label probe and provides assay performance (limit of detection of ~6 amol of an in-vitro-transcribed model target) comparable to an existing commercial bead-based technology that uses branched DNA (bDNA) signal amplification. We also demonstrate a 3-plex mRNA detection, without cross-reactivity, using shape-encoded "intraplex" hydrogel microparticles. Our ability to tune the porosity of encoded hydrogel microparticles expands the utility of this platform to now quantify biomacromolecules ranging in size from large mRNAs to small miRNAs.

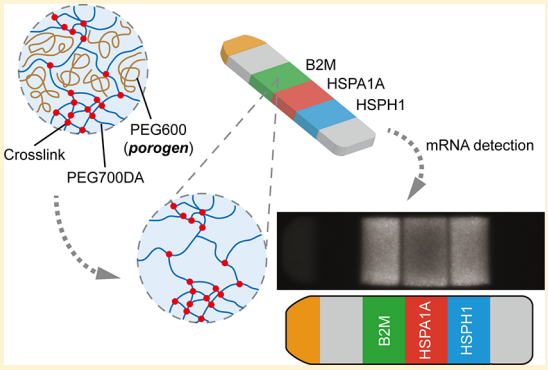

Cellular fates in physiological and pathological processes are determined by dynamic patterns of gene expression.[1−3] The quantification of gene expression for a specific set of genes, which are predictive of a disease type and response to therapy, is known as gene signature profiling. Gene signatures can be used as readouts to screen small-molecule libraries for compounds that affect intracellular pathways of interest. Specifically, applications of transcriptional profiling in cells include clinical prognosis of carcinoma,[4] monitoring responses to chemotherapy,[5] and pharmaceutical investigation of drug activities.[6] A traditional yet simple technique to quantify mRNA (mRNA) is Northern blotting, where extracted RNA samples are separated by gel electrophoresis, followed by transferring (blotting) RNA onto a nylon membrane and hybridizing with probes.[7,8] Overcoming the relatively low sensitivity of Northern blotting, reverse transcription polymerase chain reaction (RT-PCR)[2,9] has been widely used to quantify the absolute amount of mRNA from inputs as small as a single cell. Other technologies include complementary DNA (cDNA) microarrays,[10,11] RNase protection assays,[12] and nuclease protection assays.[13,14] Each method listed above has its own advantages and disadvantages: for example, the cDNA microarray and nuclease protection assays, combined with the microarray platform,[15] allow for the rapid simultaneous mapping of a very large number of mRNAs. However, an outstanding challenge is to detect and quantify patterns of mRNA expression directly, in an unbiased manner. The nuclease protection assay modifies original mRNA targets by enzymatically degrading ssRNA regions to keep RNA−DNA or RNA−RNA hybrid structures intact. The RT-PCR method requires the amplification of cDNA copies of target mRNAs. Specifically, this indirect detection of the cDNA amplicons generated from native RNA targets can cause sequence bias and skew the amplification of certain favored (or unfavored) RNA species. All of these methods could lead to potential misinterpretation of outcome data. A bead-based technology allowing for the direct detection of multiple mRNA targets without premodifying them currently appears to be the most suitable for high-throughput applications. Magnetic fluorescent Luminex microbeads coated with specific capture probes are hybridized with cell lysate to specifically capture the unamplified mRNA of interest. The quantification of the captured mRNA is done by hybridizing branched DNA (bDNA) as a signal amplifier containing up to ~400 biotin molecules, which then capture streptavidin conjugated with phycoerythrin (SA-PE).[16,17] This commercially available technology provides multiplexed detection of mRNA

Received: July 26, 2012
Accepted: September 28, 2012
Published: September 28, 2012

   dx.doi.org/10.1021/ac302128u | *Anal. Chem.* 2012, 84, 9370−9378

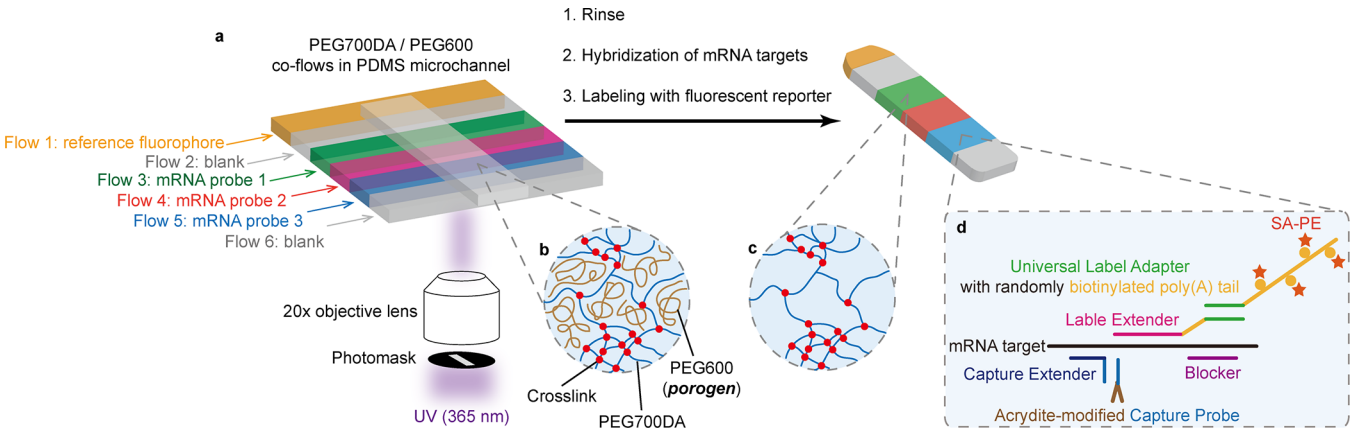

Figure 1. Schematic illustration of the hydrogel-based mRNA detection. (a) Schematic representation of synthesizing shape-coded intraplex hydrogel microparticles via stop flow lithography (SFL). Six coflows of PEG700DA and PEG600 as a porogen containing a reference fluorophore (flow 1; yellow), blanks without probes incorporated (flows 2 and 6; gray), mRNA probes (flows 2, 3, and 4; green, red, and blue), were photo-cross-linked within a PDMS microchannel by UV light (350 ± 50 nm) through a photomask and a 20× objective lens. (b and c) Schematic illustrations showing the microstructure of photo-cross-linked PEG700DA in the presence of PEG600 after UV exposure (panel (b)) and after rinsing out the porogen (panel (c)). Red dots and brown lines represent cross-links and PEG600 porogens not participating in the photo-cross-linking reaction, respectively. (d) Schematic diagram showing our hydrogel-based mRNA detection scheme. Acrydite-modified capture probe (target specific) is covalently incorporated within the bulk of the hydrogel. Multiple capture extenders (blue and dark blue line), blockers (purple line), and label extenders (pink line) containing a universal adapter (green line) are hybridized with an mRNA target (black line). A universal label probe with randomly incorporated biotins (yellow dots) on a poly(A) tail (yellow line), followed by SA-PE (red star) incubation, was used to amplify target signals.

targets up to 80 targets per well and uses a flow cytometer for post-assay analysis.[18] However, the workflow for the bDNA signal amplification requires three sequential hybridization steps with preamplifier, amplifier, and label probe, as well as rinses between the hybridization steps. In addition, total expenses could increase rapidly and become a bottleneck to perform high-throughput assays for applications in pharmaceutical research and preclinical settings.

Compared to existing plate- and bead-based technologies, poly(ethylene glycol) (PEG) hydrogel-based assay platforms have shown advantages because the PEG matrix is easy to handle and chemically conjugate desired functional groups, nonfouling, and biologically inert.[19] More remarkably, the three-dimensional (3D) mesh structure of hydrogels has been shown to enhance capture efficiency of nucleic acids.[20,21] We have recently demonstrated that lithographically encoded PEG diacrylate (PEGDA) hydrogel microparticles show significant advantages over the surface-based immobilization approaches in detecting and quantifying small fragments of DNA,[20,22] microRNAs (miRNAs),[23,24] and proteins.[19,25,26] Although PEG200 (PEG with an average molecular weight (MW) of 200) has served as an effective porogen in creating pores within the PEG700DA hydrogel microparticles, the diffusion of mRNAs typically longer than ∼1000 nt can be substantially hindered. Here, we report the quantification of unmodified full length-transcripts using PEGDA hydrogel microparticles whose effective pore size was tuned with PEG600 as an appropriate porogen. Specifically, we present (1) the synthesis and transport characterization of the porosity-tuned PEG700DA hydrogel microparticles, (2) a simpler method in both protocol and design to directly detect full-length mRNAs using a custom-designed multibiotinylated universal label probe, compared with the bDNA amplification, (3) assay performance (i.e., estimation of sensitivity and dynamic range) with an in-vitro-transcribed model target, and (4) demonstration of multiplexed detection of three mRNA targets.

EXPERIMENTAL SECTION

Fabrication of Porosity-Tuned Hydrogel Microparticles. The fabrication of hydrogel microparticles was performed via stop flow lithography (SFL), as previously described.[22−27] Briefly, PEGDA prepolymer solutions were loaded into a 38-μm-high poly(dimethylsiloxane) (PDMS, Sylgard 184, Dow Corning) channel and photo-cross-linked upon a periodic exposure of ultraviolet (UV) light (350 ± 50 nm) for 75 ms, by computer-controlled pressure valves. The UV light was transmitted by first attenuating white light from a metal-halide lamp (Lumen 200, Prior Scientific) by 39% with neutral density filters and then passing through a filter cube set (11000v3−UV; Chroma Technology Corp.). PEGDA hydrogel microparticles were synthesized at a rate of ∼5 particles/s (see Video S-1 in the Supporting Information). Two prepolymer solutions were first prepared for various regions, as shown in Figure 1a, within each microparticle as follows. PEGDA prepolymer mixture 1 consisted of 35% [v/v] PEG700DA, 20% [v/v] PEG600 porogen, 5% [v/v] Darocur 1173 photoinitiator (Sigma−Aldrich), and 40% [v/v] 3X Tris-EDTA buffer (TE, USB Corporation). PEGDA prepolymer mixture 2 consisted of 20% [v/v] PEG700DA, 40% [v/v] PEG600, 5% [v/v] photoinitiator, and 35% [v/v] 3X TE buffer. Then, a 1:9 [v/v] ratio of 0.03 mg/mL rhodamine acrylate in 1X TE was mixed with the PEGDA prepolymer mixture 1 for a reference fluorescence region (flow 1 in Figure 1a). A 1:9 [v/v] ratio of 20% [v/v] blue food coloring in 1X TE was mixed with the PEGDA prepolymer mixture 1 for blank spacer regions (flows 2 and 6 in Figure 1a). Acrydite-modified capture probes (ssDNA oligomers, Integrated DNA Technologies, IDT, Figure 1d) were dissolved in 1X TE buffer, leading to a stock concentration of 1 mM. For probe regions (flows 3, 4, and 5 in Figure 1a), each capture probe was thawed and mixed with the PEGDA prepolymer mixture 2 at a ratio of a (capture probe)/(PEGDA prepolymer mixture 2) of 1:9 [v/v] immediately before the fabrication of microparticles. Synthesized hydrogel

dx.doi.org/10.1021/ac302128u | Anal. Chem. 2012, 84, 9370−9378

microparticles were rinsed and stored in 1X TE with 0.05% [v/v] Tween-20 (TET) at 4 °C.

Porosity Characterization. The partition coefficient (K) of 500 kDa fluorescein isothiocyanate (FITC)-dextran molecule (TdB Consultancy) within 20% [v/v] PEG700DA hydrogel was estimated by allowing for its diffusion into the hydrogel and acquiring fluorescence images on an inverted microscope (Axio Observer A1, Zeiss). We used dextran as a model polymer for the transport characterization, because it behaves almost ideally in water (a Flory interaction parameter, χ = 0.48) and is commercially available. Briefly, a disk-shaped PEGDA hydrogel (diameter = 700 μm) was formed inside a PDMS microchannel (width = 2 mm, height = 40 μm) by loading a prepolymer solution containing an identical composition to the probe region for our mRNA detection (i.e., 20% [v/v] PEG700DA) in the presence of either PEG200 or PEG600 porogen, and then photo-cross-linked inside the microchannel with the same exposure of 75 ms. The size of the cylindrical hydrogel post was set by adjusting a field diaphragm that served as a photomask for the UV-cross-linking. The PDMS microchannel was fabricated by bonding a topographically patterned PDMS slab to a glass slide, both of which were chemically activated using a plasma treatment for 5 min (Plasma Cleaner PDC-32G, Harrick) prior to the attachment. Note that the plasma treatment strengthened the adhesion not only between the micropatterned PDMS slab and glass slide but also between the photo-cross-linked PEGDA hydrogel disk and top and bottom walls of the microchannel. After the photo-cross-linking, the channel was rinsed with reverse osmosis water overnight to remove unreacted prepolymers and with TET buffer prior to diffusion experiments. The fluorescently labeled dextran was dissolved in TET buffer at a fixed concentration of 2 mg/mL. Using a syringe pump, the solution was continuously delivered into the microchannel at a constant flow rate of 50 μL/h, in order to maintain a constant concentration of FITC-dextran at boundary of the cylindrical gel posts. Note that the top and bottom surfaces of the gel were adhered onto the PDMS and glass, resulting in impermeable boundaries. The dextran was left to diffuse into the hydrogel until a steady state was reached (~2 h), and then fluorescence images were acquired with an exposure time of 0.3 s. We confirmed that the temporal evolution of the radial profiles remained constant after 2 h. Fluorescent micrographs were analyzed using Matlab (Mathworks) and ImageJ (NIH). The partition coefficient (K) was calculated by dividing the average fluorescence intensity (background-subtracted) within the hydrogel post (I_{gel}) by that in the bulk solution (I_{bulk}).

In Vitro Transcription of mRNA Targets. Three mRNA targets used in this study (*Homo sapiens* beta-2-microglobulin (B2M; 987 nt), *Homo sapiens* heat shock 70 kDa protein 1A (HSPA1A; 2445 nt), and *Homo sapiens* heat shock 105 kDa/110 kDa protein 1 (HSPH1; 3680 nt)) were transcribed in vitro as follows.

(1) Each cDNA for the mRNA targets was inserted in the circular pCMV6-XL5 vector (4482 bp, OriGene). Each circular vector was reconstituted in a TE buffer to give a stock concentration of 100 ng/μL.
(2) Blunt-ended cDNAs, including the T7 promoter region, were amplified with PfuUltra II Fusion HS DNA polymerase (Agilent) and appropriately designed forward and reverse primers (18-nt ssDNA oligomers, IDT; also see Table S-1 in the Supporting Information) via polymerase chain reaction (PCR). A PCR cleaning kit (Qiagene) allowed for the purification of the amplified cDNAs including a small portion of the circular vector.
(3) Desired mRNA targets were transcribed in vitro at 37 °C for 4 h using AmpliScribe T7-*Flash* Transcription Kit (Epicenter) and purified with 5 M ammonium acetate and 70% [v/v] ethanol. The concentration of the cDNA templates and in-vitro-transcribed mRNA targets dissolved in TE buffer was estimated by measuring UV absorbance at 260 nm (Nanodrop, Thermo Scientific). The mRNA stock solutions were diluted into various concentrations (from 100 nM to 1 pM). Then, 5 μL aliquots were transferred into RNase-free microtubes and stored frozen at −20 °C prior to assays.

Design of ssDNA Oligonucleotides for Hydrogel-Based mRNA Detection. Figure 1d shows a labeling scheme of our hydrogel-based mRNA detection. Note that multiple ssDNA oligomers for capture extenders, blockers, and label extenders were used to detect an mRNA target (see Table S-2 in the Supporting Information) and hybridized on a ~500-nt-long binding region for each mRNA. Each 15-nt capture probe (light blue in Figure 1d) is complementary to capture extenders and has an acrydite modification (brown line in Figure 1d) to allow for covalent attachment to the gel. Each capture probe was designed to be specific to each mRNA target. We chose a pool of capture probes randomly from bacterial nucleotide sequences with no or minimal similarities to human genomic and transcriptional genes. An additional criterion in designing acrydite-modified capture probes was to include ~50% GC content, such that the melting temperature ranged between 50 °C and 60 °C. Second, capture extenders (20−30 nt, 5 or 6 probes per target; see the dark blue line in Figure 1d) were specific to each mRNA target and each capture probe. Third, label extenders were specific to each mRNA target (40−50 nt, 6 per target; see the pink line in Figure 1d) and had an overhang that served as a universal label adapter (28 nt; see the green line in Figure 1d). Fourth, blockers (5 or 6 per target; see the purple line in Figure 1d) were used to enhance specificity by capping unhybridized sites within the binding region. All of the probes described above were obtained from IDT (see Table S-2 in the Supporting Information).

Synthesis of Multibiotinylated Universal Label Probe. A universal label adapter (28-nt ssDNA oligomer, IDT; also see Table S-2 in the Supporting Information) whose sequence was complementary only to the 5′-end of the label extenders (the green line in Figure 1d) was first obtained. Then, the ssDNA template was extended from the 3′-end by enzymatically adding 2′-deoxyadenosine 5′-triphosphate (dATP, Life Technologies) and biotinylated dATP (biotin-14-dATP, Life Technologies) randomly with terminal transferase (New England BioLabs).[28] Specifically, 10 pmol of the universal label adapter, 2.5 nmol of dATP, and 2.5 nmol of biotin-14-dATP were mixed together in the presence of Co^{2+} ions and 20 units of the terminal transferase within the typical reaction volume of 50 μL. This 3′-end tailing was allowed to proceed at 37 °C overnight (~14 h) and stopped by adding 10 μL of 0.2 M EDTA (pH 8.0). Stock solutions were stored frozen at −20 °C prior to use.

Hydrogel-Based mRNA Assay. The hydrogel-based mRNA assay consists of three primary steps: (1) hybridization of mRNA, (2) hybridization of the universal label probe, and (3) attachment of a reporter fluorophore. For a single-plex

dx.doi.org/10.1021/ac302128u | *Anal. Chem.* 2012, 84, 9370−9378

assay as an example, 30 μL of TET buffer with 583.3 mM NaCl dissolved, 4 μL of a hydrogel microparticle suspension (~50 particles), 1 μL of a mixture of the capture extenders (1 μM each), 1 μL of a mixture of the label extenders (1 μM each), and 1 μL of a mixture of blockers (1 μM each) were added into a 0.6-mL microtube. One microliter (1 μL) of an in-vitro-transcribed mRNA target dissolved in TE was applied immediately after denaturing at 70 °C for 2 min. TET was also added to give a final assay volume of 50 μL and a final concentration of 350 mM NaCl. The assay microtube was gently vortexed prior to the hybridization at 55 °C for ~15 h with continuous agitation. We chose the hybridization period of ~15 h to compare the assay performance of our hydrogel-based with that of the bead-based assay under the same conditions. In the bead-based assay, we previously found that ~15 h served as an optimized period not only for full-length transcripts to be hybridized onto beads at steady state, but also to be suited well to the assay workflow. After the hybridization of mRNA targets, hydrogel microparticles were rinsed with 0.5 mL of 50 mM NaCl in TET three times, and additionally with 0.5 mL of 380 and 350 mM NaCl in TET to adjust the salt concentration for the hybridization of the universal label probe at 55 °C for 1 h. Then, the microparticles were rinsed with 0.5 mL of 50 mM NaCl in TET three times and incubated with 5 μL of streptavidin−phycoerythrin (SA-PE, 1 mg/mL, Invitrogen) at room temperature for 1 h. The microparticles were again rinsed as described above and resuspended in 1X TE with 0.05% [v/v] T-20 and 25% [v/v] PEG400 (PTET) prior to imaging.

Image Analysis. Hydrogel microparticles suspended in PTET were imaged between 170-μm-thick glass coverslips placed on an inverted fluorescence microscope (Axio Observer.A1, Zeiss). A metal-halide lamp (Lumen 200, Prior Scientific) was used as a white light source and filtered through a cube set (Model XF101-2, Omega Optical) for imaging orange/red fluorescence. Sixteen-bit (16-bit) fluorescence images were acquired using a CCD camera (Clara Interline CCD Camera, Andor Technology) with an exposure of 50 ms. The acquired images were then rotated, cropped, and analyzed using a custom code (Matlab, MathWorks) in a semiautomated manner. Fluorescence intensity was integrated in the probe region (~30 μm × 70 μm) for each hydrogel microparticle. Background signal was defined as integrated fluorescence intensity from microparticles hybridized with no targets. Background-subtracted median fluorescence intensity was then estimated from at least five hydrogel microparticles.

Bead-Based mRNA Assay. Affymetrix QuantiGene Plex 2.0 Assay was performed for the bead-based mRNA assay. First, a mixture of Luminex xMAP beads (magnetic fluorescent polystyrene microbeads) with target-specific capture probes incorporated on the surface were obtained. Then, the in vitro transcribed mRNA targets dissolved in TE buffer and a probe mixture containing capture extenders, label extenders, and blockers were applied into wells. The total assay volume was adjusted to 50 μL by adding either the hydrogel-based hybridization buffer (i.e., 350 mM NaCl in TET) or the Affymetrix hybridization buffer including a custom lysis mixture, proteinase K, and blocking agent provided by the vendor. Approximately 250 microbeads were used in each well. The target hybridization was at 55 °C for ~15 h with shaking. After rinsing, the amplification of signal from captured mRNA targets was applied using the branched DNA (bDNA), where the hybridization of preamplifiers, amplifiers, and biotinylated label probes occurred sequentially for 1 h each. The SA-PE incubation was combined with the last step of the bDNA amplification. Median fluorescence signal from at least 10 Luminex microbeads was determined using a flow cytometer (FLEXMAP 3D, Luminex).

Statistical Analysis. Median values of fluorescence intensity were used to capture central trends for both hydrogel- and bead-based mRNA assays. Statistical significance was assessed using the unpaired *t*-test. A value of $p < 0.05$ was considered significant.

RESULTS AND DISCUSSION

Porosity-Tuned PEGDA Hydrogel Using Porogens. We have recently demonstrated the successful quantification of miRNAs and proteins by capturing them within our standard PEGDA hydrogel microparticles synthesized with PEG200 as a porogen (PEG200 microparticles).[23−26] However, we found that the standard hydrogel microparticles did not have large enough pores to capture full-length mRNA transcripts, largely due to significant steric hindrance resulting from their size relative to the effective pore size of the PEG200 microparticles. Yoffe et al.[29] have shown that the average maximum ladder distance (⟨MLD⟩) can be used as a measure of the extendedness of RNA secondary structures, including single-stranded (ss) loops (i.e., hairpin, bubble, bulge, or multi-branch). Based on this assumption, the radius of gyration (R_g) of ss-mRNAs scales as $R_g \approx \overline{\langle MLD \rangle}^{0.5} = (0.485N^{0.68})^{0.5} \approx N^{0.34}$, which is also similar to another estimation[30] based on the Flory scaling law: $R_g \approx 0.55N^{1/3}$, where N is the number of nucleotides. Estimated radii of gyration of the three mRNA targets used in this study ranged from 7 nm to 11 nm (Table 1). For comparison, estimated radii of typical mature miRNAs were ~3 nm. Werner[31] has recently shown that the size of various tRNA and rRNA molecules (54−226 nt) ranged from 2 nm to 5 nm. For another comparison, the hydrodynamic radii of the tumor necrosis factor (TNF; 52 kDa) and IgG (150 kDa)—typical cytokine and globular protein—are 3.1 and 5.3 nm, respectively.[32,33] Recently, Lee et al.[34,35] have showed that macroporosity in 5% [w/v] PEG700DA hydrogels can be generated by polymerization-induced phase separation,[36] in the presence of PEG porogens with molecular weight ranging from 3400 to 35 000. They demonstrated that over 60% of 250 kDa FITC-dextran diffused into the PEGDA hydrogel at equilibrium.[34] They have also recently showed that the macroporosity allowed for increased sensitivity in detecting kinase activity from cell lysates.[35] Others have also presented detailed experimental evidence that aqueous solutions of PEGDA undergo polymerization-induced phase separation.[37,38]

Table 1. Estimated Radii of Gyration of mRNA Targets Used in This Study

mRNA	number of nucleotides, N [nt]	calculated R_g [nm]
B2M	987	7.3
HSPA1A	2383	10
HSPH1	3680	11

Figure 2a shows that the PEG600 porogen resulted in enhanced capture efficiency, compared with PEG200, by a factor of ~8 when 1 fmol of HSPA1A (2383 nt) was hybridized and labeled with a single-biotinylated universal probe and SA-PE in shape-coded Janus microparticles (left photo-cross-linked with PEG200 and right with PEG600; see frame (i) in Figure

dx.doi.org/10.1021/ac302128u | Anal. Chem. 2012, 84, 9370−9378

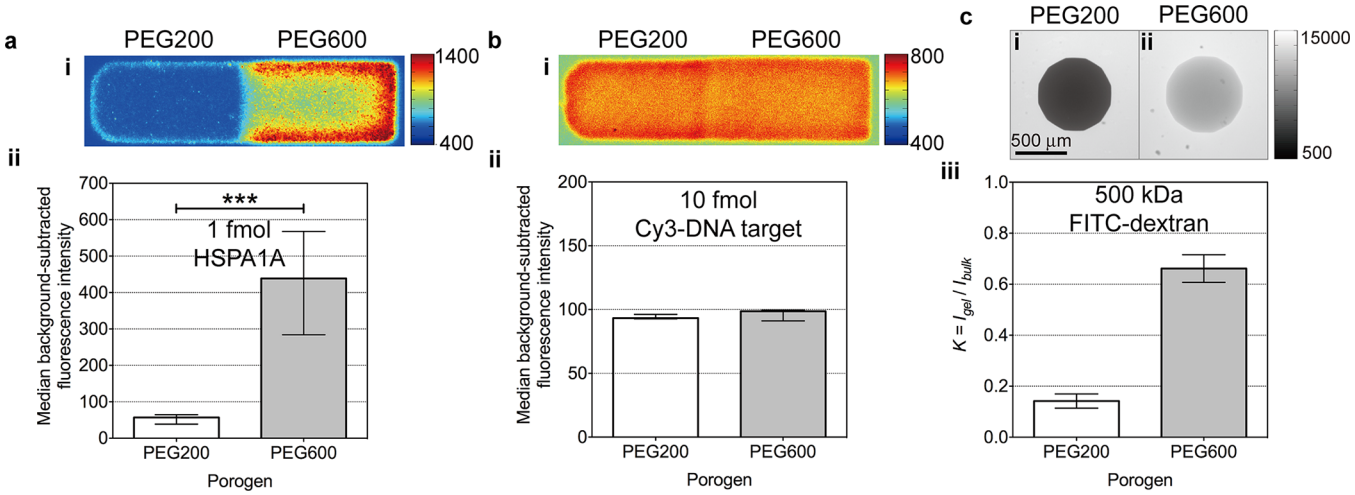

Figure 2. Comparison of PEG200 and PEG600 porogens. (a) Comparison between PEG200 and PEG600 porogens for the hydrogel-based mRNA detection. Frame (i) shows a fluorescence micrograph depicting a representative Janus hydrogel microparticle for the detection of 1 fmol of HSPA1A, labeled with SA-PE; the left and right halves that were photo-cross-linked in the presence of PEG200 and PEG600 porogens, respectively. Frame (ii) shows a bar graph depicting median values of background-subtracted fluorescence intensity in the two regions; error bars are interquartile ranges (n = 8). [The three-asterisk symbol set (***) denotes the statistical difference (p < 0.0001).] (b) Comparison between PEG200 and PEG600 porogens for the incorporation efficiency of a ssDNA-oligomer probe. Frame (i) shows a fluorescence micrograph depicting a representative Janus hydrogel microparticle for the detection of 10 fmol of Cy3-conjugated DNA target (20 nt), whereas frame (ii) shows a bar graph depicting median values of background-subtracted fluorescence intensity in PEG200 and PEG600 regions (error bars are interquartile ranges (n = 7)). (c) Comparison between PEG200 and PEG600 porogens for the diffusion of FITC-dextran. Fluorescence micrographs showing 500 kDa FITC-dextran (Stokes' radius of 14.7 nm) diffused into 20% [v/v] PEG700DA cylindrical posts photo-cross-linked with PEG200 (frame (i)) and PEG600 (frame (ii)) at 128 min. Frame (iii) shows a bar graph representing the partition coefficients of 500 kDa FITC-dextran in the PEGDA posts at 128 min (here, error bars represent the standard deviation (102 data points, radially averaged within each PEGDA post, were analyzed)).

2a). To confirm that the resulting change in capture efficiency was not a consequence of different amounts of capture probes incorporated within the hydrogels, we used the same type of Janus microparticles to hybridize a small (20-nt) DNA target conjugated with Cy3 fluorophore. Figure 2b shows that fluorescence signals from the two regions were almost identical. These observations indicate that PEG600 served as an efficient porogen in both increasing the effective pore size and capturing the relatively large mRNA target without compromising the incorporation efficiency of acrydite-modified capture probes. We further confirmed that the enhanced capture efficiency of the mRNA target resulted from the increased porosity of hydrogel by comparing the diffusion of a nonreactive molecule (dextran) into cylindrical posts cross-linked inside a PDMS microchannel, as described in the Experimental Section. We chose 500 kDa FITC-dextran (Stokes' radius of 14.7 nm), since its size was similar to that of the mRNA targets (10−11 nm). We measured the partition coefficient (K) of the FITC-dextran (Figure 2c) and found that the value of K for the hydrogel cross-linked with PEG600 porogen was ∼4.7 times larger (K_{PEG600} = 0.66 ± 0.05) than that with PEG200 (K_{PEG200} = 0.14 ± 0.03). We also observed that diffusion of 500 kDa FITC-dextran into the hydrogel cross-linked with PEG600 porogen was faster, in comparison to the PEG200 porogen, and that the hydrogel cross-linked with PEG200 porogen remained relatively almost impermeable to the FITC-dextran for ∼9 h (see Figure S-1 in the Supporting Information). The large pores generated by the PEG600 porogen is associated with the polymerization-induced phase separation occurring at a larger length scale, when compared with the PEG200 porogen. Note that PEGDA hydrogel particles cross-linked with PEG600 porogen were more opaque than those fabricated with PEG200 (see Figure S-2 in the Supporting Information), which is consistent with their relative porosity and suggests that pores with dimensions of hundreds of nanometers were created. These experimental data suggest that our choice of PEG600 as a porogen allowed for the increased porosity of photo-cross-linked 20% [v/v] PEG700DA hydrogel and therefore significantly enhanced permeation of larger macromolecules while maintaining structural integrity of the hydrogel constructs used in our study.

We also tried PEG6000 as a porogen, but a prepolymer solution containing 20% [v/v] PEG700DA and 40% [v/v] PEG6000 appeared to be phase-separated macroscopically before the photo-cross-linking process. Although decreasing the volume fraction of PEG6000 down to 20% [v/v], and increasing that of PEG700DA to 35% [v/v], prevented the macroscopic phase separation in the prepolymer solution, the detection efficiency of HSPA1A in the resulting hydrogel was substantially lower, when compared to the PEG600 porogen particles (see Figure S-3 in the Supporting Information). This difference is likely to be attributed to a higher cross-linking density and lower porosity due to the change in volume fractions of PEG700DA and PEG porogens (i.e., 1.75 PEG700DA:1 PEG6000 vs 1 PEG700DA:2 PEG600). In addition, the accessibility of a target molecule into PEGDA immobilized with a probe could decrease as the molecular weight of porogens increases.[34] More specifically, while polymerization-induced phase separation occurs, the PEG6000 porogen could result in more-favorable incorporation of the acrydite-modified capture probe within PEGDA-rich domains where the capture probe becomes less accessible to the mRNA target and other labeling components (e.g., SA-PE). These results demonstrate that relative portions and miscibility of PEGDA and PEG porogens, as well as molecular weight of

dx.doi.org/10.1021/ac302128u | Anal. Chem. 2012, 84, 9370−9378

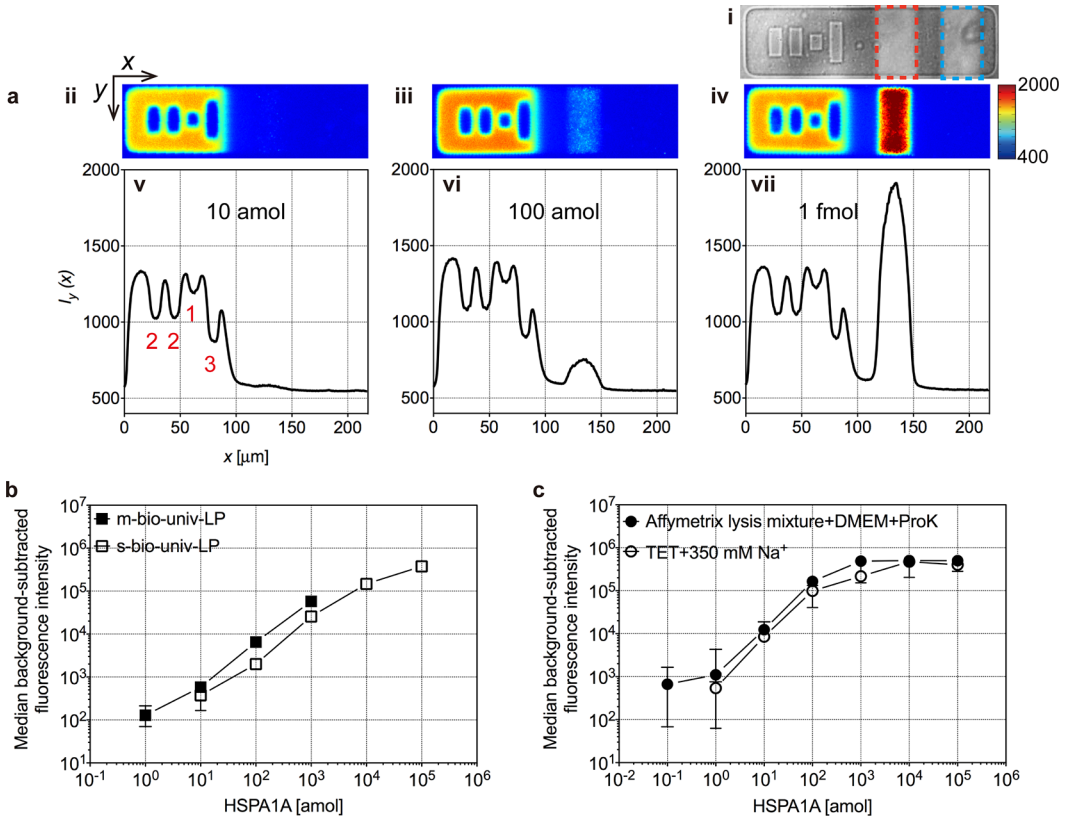

Figure 3. Quantification of in-vitro-transcribed HSPA1A using the porosity-tuned hydrogel microparticles. (a) Frame (i) shows a bright-field snapshot of a barcoded (code 3122) hydrogel microparticle being synthesized during stop flow lithography (SFL) (also see Video S-2 in the Supporting Information), containing HSPA1A-specific capture probe incorporated (red dotted box) and no capture probe (blue dotted box); the three dark bands are blank spacers containing the food coloring dye. Also shown are fluorescence micrographs of representative hydrogel microparticles after detecting 10 amol (frame (ii)), 100 amol (frame (iii)), and 1 fmol (frame (iv)) of in-vitro-transcribed HSPA1A, labeled with multibiotinylated label probe, followed by SA-PE incubation. Plots of spatially resolved *y*-averaged fluorescence intensity along the *x*-direction for the microparticles shown in frames (ii)−(iv) are given in frames (v)−(vii). (b) Calibration curves showing median values of integrated, background-subtracted fluorescence intensity within the probe region (red dotted box in frame (i) in panel (a)) for the hydrogel-based quantification of various amounts of in-vitro-transcribed HSPA1A, labeled with multibiotinylated label probe (filled squares) and single-biotinylated label probe (open squares). Error bars are interquartile ranges (n = 10−14). (c) Calibration curves showing median values of integrated, background-subtracted fluorescence intensity from Luminex microbeads for the same target as presented in panels (a) and (b). The hybridization of the target was performed in either a lysis mixture provided by Affymetrix (filled circles) or 350 mM NaCl in TET (open circles). Error bars are interquartile ranges (n = 3−5).

PEG porogens, are important factors to consider in tuning the effective porosity of PEGDA hydrogel constructs.

Quantification of In-Vitro-Transcribed mRNA Model Target Using Porosity-Tuned Hydrogel Microparticles. We present a relatively simple scheme to amplify signal using a multibiotinylated universal label probe, as illustrated in Figure 1d for the quantification of mRNA. To verify our detection and amplification schemes, we used lithographically encoded PEGDA microparticles (code 3122 as shown in Figure 3a, frame (i)) and HSPA1A as a model target. Frame (i) in Figure 3a shows a bright-field image of the barcoded microparticle containing a probe region where an acrydite-modified capture probe for HSPA1A was incorporated (see the red dotted box in Figure 3a, frame (i)) and a negative control region without the capture probe incorporated (denoted as the blue dotted box in Figure 3a, frame (i)). We found no nonspecific binding of HSPA1A in the control region (see frames (ii)−(iv) in Figure 3a). We also tried hybridizing both HSPA1A and a nonspecific target (B2M) simultaneously and observed no nonspecific binding. After hybridizing the multibiotinylated universal label probe and SA-PE sequentially to amplify the target signal, we acquired fluorescence images of at least five microparticles from each amount of spiked in-vitro-transcribed HSPA1A (1, 10, 100, or 1000 amol), as shown in panels (ii)−(iv) in Figure 3a. Then, we calculated the *y*-averaged fluorescence intensity to generate corresponding spatially resolved fluorescence profiles along the *x*-direction (see frames (v)−(vii) in Figure 3a). Figure 3b shows calibration curves obtained with the signal amplification (filled squares) and no signal amplification using the single-biotinylated universal label probe (open squares). Our signal amplification with the multibiotinylated universal label probe showed a limit of detection (LOD) of 6.4 amol, defined as an estimated target amount when signal-to-noise ratio (S/N) is 3, and a linear signal response (R^2 = 0.98, also see Table 2) over 3 logarithmic units (see red squares in Figure 3b). With the single-biotinylated universal label probe, the LOD was found to be 33 amol with a similar dynamic range. To benchmark our hydrogel-based mRNA quantification, we performed a commercially available bead-based assay with the same model target. Calibration curves obtained from two assay conditions (one with the same hybridization buffer used for the hydrogel-based assay and the other with a standard hybrid-

dx.doi.org/10.1021/ac302128u | *Anal. Chem.* 2012, 84, 9370−9378

Table 2. Limit of Detection for the Hydrogel- and Bead-Based Assays

	limit of detection
Hydrogel-Based mRNA Assay	
multibiotinylated universal label probe	6.4 amol
single-biotinylated universal label probe	33 amol
Bead-Based mRNA Assay	
hydrogel hybridization buffer	2.1 amol
Panomics hybridization buffer	1.1 amol

ization buffer provided by Affymetrix) show almost the same assay performance (Figure 3c). The dynamic ranges of both hydrogel- and bead-based assays were determined to be similar, and the sensitivity of the hydrogel-based assay, represented by the LOD, appeared to be comparable to the existing technology. The performances of the two types of assays are summarized in Table 2.

While the bDNA amplification used in the bead-based assay (three hybridization steps with preamplifier, amplifier, and biotinylated label probe sequentially)[16,39] could offer a theoretical amplification factor of ~400 per bDNA, our simple scheme to amplify signal (i.e., only 1 hybridization step with the multibiotinylated universal label probe) allowed for comparable assay performance without requiring the complex structures employed by the bDNA amplification. Although it is not easy to directly compare the detection and labeling efficiency of the hydrogel- and bead-based assays, we can define maximum amplification density, $\rho_{max,amp}$ accounting for (1) the total number of possible sites where the binding of biotin and SA-PE occurs ($N_{biotin-SAPE}$), and (2) the projected area on which acrydite-modified capture probes are incorporated (A_p):

$$\rho_{max,amp}\ [\mu m^{-2}] \equiv \frac{N_{biotin-SAPE}}{A_p} = \frac{(n_{label\ probe})(n_{biotin-SAPE,\ probe})}{(\pi/4)d_e^{\,2}} \quad (1)$$

where $n_{label\ probe}$ is the number of label probes used for an mRNA target, and $n_{biotin-SAPE,\ probe}$ is the number of possible binding sites per label probe. The parameter d_e is the equivalent spherical diameter of a particle (either the probe region within a hydrogel microparticle or the Luminex microbead), defined as $d_e = (6V_p/\pi)^{1/3}$, where V_p is the volume of the particle. The parameter $d_{e,Luminex}$ is equal to 5.6 μm, assuming that the Luminex microbead is a perfect sphere, and $d_{e,\ hydrogel}$ = 53 μm for the probe region (rectangular cuboid; 30 μm × 70 μm × 38 μm). The maximum labeling density includes two major components: (1) an amplification factor, represented by $N_{biotin-SAPE}$, and (2) a capture efficiency factor (A_p). With $n_{biotin-SAPE,\ probe}$ = 6 for both types, $n_{biotin-SAPE,\ hydrogel}$ = 5 and $n_{biotin-SAPE,\ Luminex}$ = 400, $\rho_{max,amp,\ Luminex}/\rho_{max,amp,\ hydrogel}$ is 7279. Although $\rho_{max,amp}$ of the bead-based assay appears to be much larger, the estimated LOD value of our hydrogel-based detection with the multibiotinylated universal label probe was

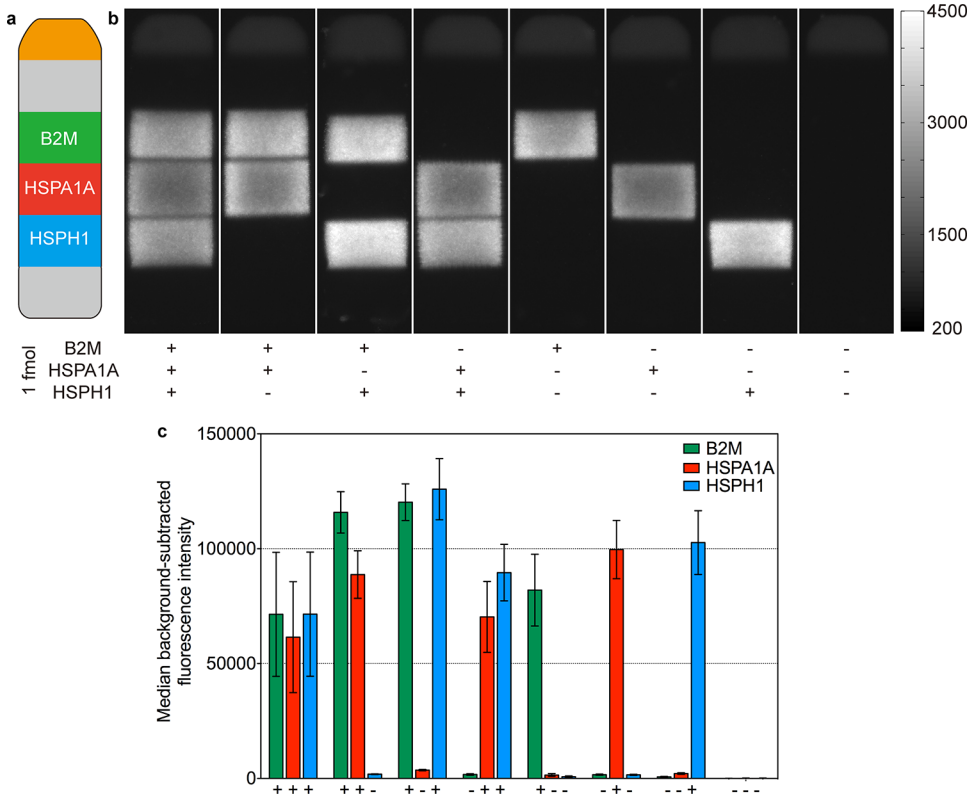

Figure 4. Demonstration of 3-plex mRNA assay using intraplex hydrogel microparticles. (a) Schematic illustration of shape-coded intraplex hydrogel microparticle consisting of reference fluorophore region (orange), two blank regions (gray), and three probe regions for B2M (green), HSPA1A (red), and HSPH1 (blue). (b) Fluorescence micrographs showing representative microparticles after simultaneously detecting various combinations of 1 fmol B2M, HSPA1A, and HSPH1 spiked-in samples. The symbols "+" and "−" denote the presence and absence of each target, respectively. (c) Bar graph showing mean values of background-subtracted fluorescence intensity in the three probe regions. Error bars represent standard deviation (n = 5−9).

dx.doi.org/10.1021/ac302128u | Anal. Chem. 2012, 84, 9370−9378

within an order of magnitude of the LOD obtained with the bead-based assay. This capture/label conflation is attributed to the larger capture efficiency for the hydrogel-based assay ($A_{p,\ \mathrm{hydrogel}}/A_{p,\ \mathrm{Luminex}} = 91$) and the larger amplification factor for the bead-based assay ($N_{\mathrm{biotin-SAPE,\ Luminex}}/N_{\mathrm{biotin-SAPE,\ hydrogel}} = 80$). An additional factor that is not introduced explicitly in eq 1 should be also considered: the thermodynamically more favored environment (i.e., smaller dissociation constant or Gibbs free energy change between probes and targets) within hydrogel. This thermodynamic factor is attributed to enhanced binding stability between targets and capture probes within three-dimensional (3D) (conformationally more favorable) hydrogel structures.[20] Further optimization in the signal amplification by either increasing the number of biotins incorporated on the multibiotinylated label probe or applying the recently presented rolling circle amplification (RCA)[23] to the mRNA quantification could lead to substantial enhancements in assay performance. Such improvement has the potential to open new opportunities in profiling physiologically or pathologically important mRNAs whose copy numbers are inherently very low.

Demonstration of 3-plex mRNA Assay Using Intraplex Hydrogel Microparticles. The detection of multiple analytes simultaneously has been of great interest, particularly in the pharmaceutical research field toward screening drug candidate compounds. To demonstrate extended applicability of our hydrogel-based mRNA detection, we performed a 3-plex mRNA assay with shape-coded hydrogel microparticles containing three probe regions (see Figures 1 and 4a). Figure 4b shows that several combinations of 1 fmol B2M, HSPA1A, and HSPH1 were successfully captured without cross-reactivity, whereas none of the targets appeared to be detected with PEG200 as a porogen (also see Figure 2a for a side-by-side comparison). Fluorescence signal levels of spiked-in mRNA targets in each combination were similar, although slight variations in signal for each target appeared in the different conditions (Figure 4c). More interestingly, we observed very clear interfaces between the probe regions consecutively located within the "intraplex" microparticles, despite the absence of blank spacer regions (Figure 4b). These interprobe zones were ~4 μm over which the concentration gradient of capture probes occurred, because of the lateral diffusion during SFL cycles, specifically, a stop time of 0.2 s. Since the concentration of each capture probe decreases rapidly to zero in the interprobe zones, the probability to capture large mRNA targets could also decrease substantially by the fact that multiple (five or six) capture probes were required. These interprobe zones are practically beneficial in analyzing fluorescence signals, because they serve effectively as blank areas and allow for easier identification of individual probe regions.

CONCLUSIONS

We have demonstrated successful quantification of full-length mRNAs using porosity-tuned PEG700DA hydrogel microparticles synthesized via SFL. Compared with PEG200 as our standard porogen, PEG600 allowed for significantly enhanced mass transport of mRNA targets (R_g > 7 nm) during hybridization within the bulk of PEGDA hydrogel while the incorporation efficiency of an acrydite-modified capture probe remained almost the same. Diffusion of 500 kDa FITC-dextran (Stokes' radius of 14.7 nm) into PEG700DA cylindrical posts photo-cross-linked with either PEG200 or PEG600 porogen suggests that heterogeneous microphase separation could result in a significantly increased partition coefficient within the PEG600 post. We showed that our relatively simple hydrogel-based mRNA detection scheme with a multibiotinylated universal label probe allowed for comparable assay performance, compared with an existing bead-based technology in which bDNA signal amplification was used. We also successfully demonstrated the 3-plex mRNA detection without cross-reactivity using shape-coded intraplex hydrogel microparticles. We note that autonomously clear interprobe zones appeared after the detection and these clear zones serve as practically useful blank regions for easier signal analysis. Further investigation to improve the signal amplification, for example, by increasing the incorporation efficiency of biotins on the universal label probe or applying RCA[23,40] could allow for the quantification of mRNA targets directly from small amounts of cell lysates or blood samples. Finally, our ability to tune the porosity of PEGDA hydrogel microparticles introduces the opportunity to quantify of various types of biomolecules ranging from large mRNAs to small miRNAs simultaneously, which could aid in clinical prognosis and diagnosis, and in screening drug compounds.

ASSOCIATED CONTENT

Supporting Information

Additional information as noted in text. This material is available free of charge via the Internet at http://pubs.acs.org.

AUTHOR INFORMATION

Corresponding Author

*E-mail addresses: pdoyle@mit.edu (P.S.D.), adam.hill@novartis.com (W.A.H.).

Present Addresses

[§]Center for BioMicrosystems, Brain Science Institute, Korea Institute of Science and Technology (KIST), Seoul 136−791, Korea.

[#]Department of Chemical and Biomolecular Engineering, Sogang University, Seoul 121−742, Korea.

Notes

The authors declare no competing financial interest.

ACKNOWLEDGMENTS

This work was supported by Novartis Institutes for Biomedical Research (NIBR) Presidential Fellowship and NIBR Education Office. We thank Ki Wan Bong, Rathi L. Srinivas, and David C. Appleyard for helpful discussion.

REFERENCES

(1) Bakstad, D.; Adamson, A.; Spiller, D. G.; White, M. R. H. *Curr. Opin. Biotechnol.* **2012**, *23*, 103−109.

(2) Bustin, S. A. *J. Mol. Endocrinol.* **2000**, *25*, 169−193.

(3) Schwanhausser, B.; Busse, D.; Li, N.; Dittmar, G.; Schuchhardt, J.; Wolf, J.; Chen, W.; Selbach, M. *Nature* **2011**, *473*, 337−342.

(4) Ihmann, T.; Liu, J. A.; Schwabe, W.; Hausler, P.; Behnke, D.; Bruch, H. P.; Broll, R.; Windhovel, U.; Duchrow, M. *J. Cancer Res. Clin. Oncol.* **2004**, *130*, 749−756.

(5) Desjardin, L. E.; Perkins, M. D.; Wolski, K.; Haun, S.; Teixeira, L.; Chen, Y.; Johnson, J. L.; Ellner, J. J.; Dietze, R.; Bates, J.; Cave, M. D.; Eisenach, K. D. *Am. J. Respir. Crit. Care Med.* **1999**, *160*, 203−210.

(6) Ji, R. R.; de Silva, H.; Jin, Y. S.; Bruccoleri, R. E.; Cao, J.; He, A. Q.; Huang, W. J.; Kayne, P. S.; Neuhaus, I. M.; Ott, K. H.; Penhallow, B.; Cockett, M. I.; Neubauer, M. G.; Siemers, N. O.; Ross-Macdonald, P. *PLoS Comput. Biol.* **2009**, 5.

(7) Streit, S.; Michalski, C. W.; Erkan, M.; Kleeff, J.; Friess, H. *Nat. Protoc.* **2009**, *4*, 37−43.

(8) Alwine, J. C.; Kemp, D. J.; Stark, G. R. *Proc. Natl. Acad. Sci. U. S. A.* **1977**, *74*, 5350−5354.
(9) Weis, J. H.; Tan, S. S.; Martin, B. K.; Wittwer, C. T. *Trends Genet.* **1992**, *8*, 263−264.
(10) Schena, M.; Shalon, D.; Davis, R. W.; Brown, P. O. *Science* **1995**, *270*, 467−470.
(11) Ramsay, G. *Nat. Biotechnol.* **1998**, *16*, 40−44.
(12) Hod, Y. *Biotechniques* **1992**, *13*, 852−854.
(13) Pechhold, S.; Stouffer, M.; Walker, G.; Martel, R.; Seligmann, B.; Hang, Y.; Stein, R.; Harlan, D. M.; Pechhold, K. *Nat. Biotechnol.* **2009**, *27*, 1038−U106.
(14) Calzone, F. J.; Britten, R. J.; Davidson, E. H. *Method Enzymol.* **1987**, *152*, 611−632.
(15) Bourzac, K. M.; Rounseville, M. P.; Zarate, X.; Maddula, V.; Henderson, D. C.; Luckey, J. A.; Seligmann, B.; Galbraith, D. W. *J. Biotechnol.* **2011**, *154*, 68−75.
(16) Ching, L. K.; Mompoint, F.; Guderian, J. A.; Picone, A.; Orme, I. M.; Coler, R. N.; Reed, S. G.; Baldwin, S. L. *J. Immunol. Methods* **2011**, *373*, 54−62.
(17) Zhang, A. G.; Pastor, L.; Nguyen, Q.; Luo, Y. L.; Yang, W.; Flagella, M.; Chavli, R.; Bui, S.; Nguyen, C. T.; Zheng, Z.; He, W. H.; McMaster, G.; Witney, F. *J. Biomol. Screen* **2005**, *10*, 549−556.
(18) http://www.panomics.com/product/6/, accessed Oct. 10, 2012.
(19) Appleyard, D. C.; Chapin, S. C.; Srinivas, R. L.; Doyle, P. S. *Nat. Protoc.* **2011**, *6*, 1761−1774.
(20) Pregibon, D. C.; Doyle, P. S. *Anal. Chem.* **2009**, *81*, 4873−4881.
(21) Fotin, A. V.; Drobyshev, A. L.; Proudnikov, D. Y.; Perov, A. N.; Mirzabekov, A. D. *Nucleic Acids Res.* **1998**, *26*, 1515−1521.
(22) Pregibon, D. C.; Toner, M.; Doyle, P. S. *Science* **2007**, *315*, 1393−1396.
(23) Chapin, S. C.; Doyle, P. S. *Anal. Chem.* **2011**, *83*, 7179−7185.
(24) Chapin, S. C.; Appleyard, D. C.; Pregibon, D. C.; Doyle, P. S. *Angew. Chem.-Int. Edit.* **2011**, *50*, 2289−2293.
(25) Srinivas, R. L.; Chapin, S. C.; Doyle, P. S. *Anal. Chem.* **2011**, *83*, 9138−9145.
(26) Appleyard, D. C.; Chapin, S. C.; Doyle, P. S. *Anal. Chem.* **2011**, *83*, 193−199.
(27) Bong, K. W.; Chapin, S. C.; Pregibon, D. C.; Baah, D.; Floyd-Smith, T. M.; Doyle, P. S. *Lab Chip* **2011**, *11*, 743−747.
(28) Flickinger, J. L.; Gebeyehu, G.; Buchman, G.; Haces, A.; Rashtchian, A. *Nucleic Acids Res.* **1992**, *20*, 2382−2382.
(29) Yoffe, A. M.; Prinsen, P.; Gopal, A.; Knobler, C. M.; Gelbart, W. M.; Ben-Shaul, A. *Proc. Natl. Acad. Sci. U. S. A.* **2008**, *105*, 16153−16158.
(30) Rawat, N.; Biswas, P. *Phys. Chem. Chem. Phys.* **2011**, *13*, 9632−9643.
(31) Werner, A. *Nucleic Acids Res.* **2011**, 39.
(32) Kohno, T.; Tam, L. T. T.; Stevens, S. R.; Louie, J. S. *J. Invest. Dermatol. Symp. Proc.* **2007**, *12*, 5−8.
(33) Armstrong, J. K.; Wenby, R. B.; Meiselman, H. J.; Fisher, T. C. *Biophys. J.* **2004**, *87*, 4259−4270.
(34) Lee, A. G.; Arena, C. P.; Beebe, D. J.; Palecek, S. P. *Biomacromolecules* **2010**, *11*, 3316−3324.
(35) Lee, A. G.; Beebe, D. J.; Palecek, S. P. *Biomed. Microdevices* **2012**, *14*, 247−257.
(36) Dusek, K. *Polym. Lett.* **1965**, *3*, 209−212.
(37) Wu, Y. H.; Park, H. B.; Kai, T.; Freeman, B. D.; Kalika, D. S. *J. Membr. Sci.* **2010**, *347*, 197−208.
(38) Ju, H.; McCloskey, B. D.; Sagle, A. C.; Wu, Y. H.; Kusuma, V. A.; Freeman, B. D. *J. Membr. Sci.* **2008**, *307*, 260−267.
(39) Gnatenko, D. V.; Zhu, W.; Bahou, W. F. *Thromb. Haemost.* **2008**, *100*, 929−936.
(40) Murakami, T.; Sumaoka, J.; Komiyama, M. *Nucleic Acids Res.* **2012**, 40.